Magnetocrystalline Anisotropy in Glancing Angle Deposited Permalloy Nanowire Arrays

G. Mankey – University of Alabama

et al.

Citation of published version:

Alouach, H., Fujiwara, H., Mankey, G. (2005): Magnetocrystalline Anisotropy in Glancing Angle Deposited Permalloy Nanowire Arrays. *Journal of Vacuum Science and Technology A*, 23(4). DOI: https://doi.org/10.1116/1.1938978

Magnetocrystalline anisotropy in glancing angle deposited Permalloy nanowire arrays

H. Alouach, H. Fujiwara, and G. J. Mankey[a)]
Center for Materials for Information Technology and Department of Physics and Astronomy, The University of Alabama, Tuscaloosa, Alabama 35487-0209

(Received 6 October 2004; accepted 25 April 2005; published 28 June 2005)

The magnetic anisotropy and properties of Permalloy ($Ni_{80}Fe_{20}$) nanowire arrays fabricated by glancing angle deposition with substrate rotation were studied. Epitaxial Cu nanowires, with the long axis textured along the Cu[111] crystallographic direction, were used as a seed layer to grow the $Ni_{80}Fe_{20}$ nanowires. The nanowires exhibit a strong $Ni_{80}Fe_{20}$[311] texture as shown by x-ray diffraction, with a $Ni_{80}Fe_{20}$[111] diffraction peak uniformly distributed about the wire's long axis normal to the substrate. Hysteresis loops taken at different angular orientations show that the magnetization saturates first along the wire's growth direction normal to the substrate. Samples with an aspect ratio of approximately one have equal in- and out-of-plane coercivity. At low aspect ratios ($\sim$0.5–1.5), the angular dependence of the remanence shows that the maximum remanence lies on the surface of a cone with its axis along the substrate normal. A model which contains biaxial anisotropy with a symmetry axis normal to the substrate was found to qualitatively explain the characteristics of the observed hysteresis loops. An anisotropy constant on the order of 10^6 erg/cc is necessary to explain the observed behavior, which is much larger than that of bulk $Ni_{80}Fe_{20}$.
 [DOI: 10.1116/1.1938978]

I. INTRODUCTION

Nanowire crystallographic growth orientation depends on the choice of substrate, substrate preparation, and the deposition parameters. For example, Cu nanowires grown on native oxide Si(100) at a deposition angle of 75° with substrate rotation have a strong Cu(110) texture along the wire long axis with the corresponding Cu(111) directions uniformly distributed in the azimuthal direction.[1] The Cu(111) plane is the low energy surface orientation of fcc Cu. By contrast, Cu nanowires deposited on hydrogen terminated Si(110), otherwise using the same deposition parameters, have an epitaxial orientation relationship to the substrate with the Cu(111) plane parallel to the substrate plane.[2] However, beyond the critical height for epitaxial growth, a Cu(311) texture develops with the corresponding Cu(111) directions uniformly distributed in the azimuthal direction.

There are many applications of GLAD structures depending on the material specifications.[3,5] For example, magnetic nanowires with high aspect ratios have a strong magnetic shape anisotropy[6] which makes them potential candidates for data storage and spintronic applications. The performance of devices based on spin transport mechanisms has a strong dependence on the crystallography, so it is useful to develop techniques that control the crystallography.

II. EXPERIMENT

Si(110) substrates were deoxidized and hydrogen terminated by dipping in 5% diluted hydrofluoric acid for about 15 min. Cu nanowire arrays were then deposited on this surface with the incident flux at a polar angle of 75° while rotating the substrate at an azimuthal rotation rate of 0.01 rotations/s. Cu was deposited using electron beam evaporation at a rate of 0.5 nm/s. The pressure was in the upper range of 10^{-7} Torr. Under these conditions, the Cu nanoarrays grow epitaxially up to a critical height of about 300 mm^2. The deposited layer thickness was determined by including the geometric factor for the polar inclination of the substrate relative to the incident flux direction. The Cu thickness used in this experiment is 200 nm.

The Cu nanoarrays were used as a template for subsequent growth of the $Ni_{80}Fe_{20}$ nanowires. By using Cu nanoarrays as seed layers, we intend to inhibit the formation of a more or less continuous layer of $Ni_{80}Fe_{20}$ at the beginning of the growth process to reduce magnetic coupling between the wires. With the exception of the deposition rate (0.4 nm/s), the deposition parameters remained unchanged. Thicknesses ranging from 50 to 300 nm were deposited and the structure was characterized using x-ray diffraction and scanning electron microscopy (SEM).

For the magnetic characterization, a vibrating sample magnetometer was used to determine the anisotropy and magnetization switching behavior of the nanowire arrays. The magnetic anisotropy was determined by measuring the remanent magnetization as a function of the magnetic field orientation relative to the wire long axis. Then, hysteresis loops along the magnetization easy and hard directions were measured. A detailed description of the sample's polar and azimuthal orientation with a schematic is described elsewhere.[1]

III. RESULTS

Figure 1 is a planar view scanning electron microscopy image of nanowire arrays consisting of 200 nm Cu seed lay-

a)Electronic mail: gmankey@mint.ua.edu

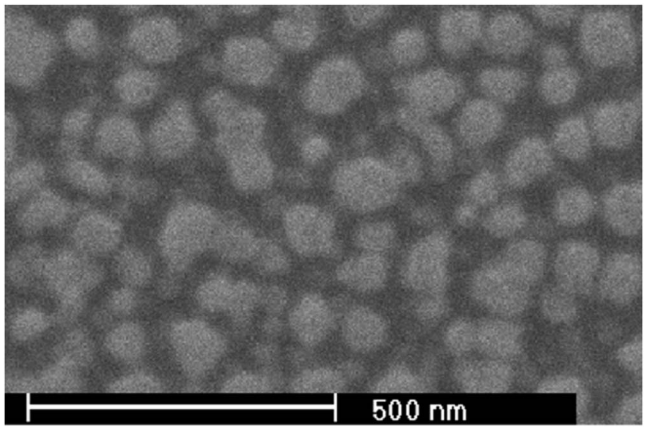

FIG. 1. Planar view scanning electron microscopy image of nanoarrays consisting of 200 nm Cu seed layers and 100 nm $Ni_{80}Fe_{20}$ deposited using GLAD at 75°. The average size is about 90 nm.

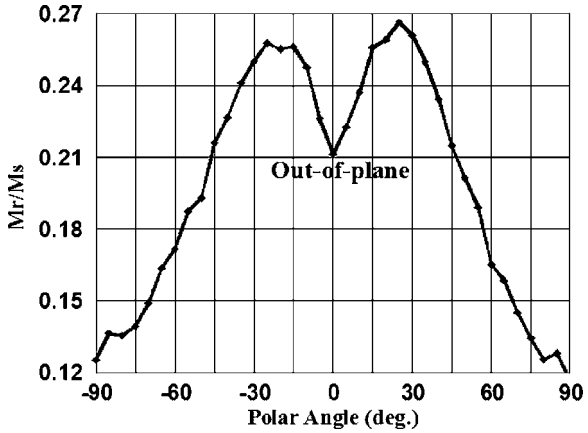

FIG. 2. Remanent magnetization of 100 nm $Ni_{80}Fe_{20}$ nanoarrays as a function of the polar angle. Since measurements for different azimuthal orientations of the sample yield identical results, it is suggested that the easy axes are distributed on a conical surface with the symmetric axis normal to the substrate plane.

ers and 100 nm $Ni_{80}Fe_{20}$. The average linear dimension of the features is about 90 nm. Previous experiments[7] have shown that the cross sectional area of the columns increases with the thickness. For samples with a thickness larger than 300 nm, SEM images showed that the top of the adjacent wires join together to form a more or less continuous structure. Thus, only samples with thicknesses less than 300 nm that yield samples with distinct wires were characterized.

X-ray diffraction scans in the $\theta-2\theta$ mode on $Ni_{80}Fe_{20}$ nanowire arrays grown onto the top of arrays of epitaxial Cu(111) nanowires, show that the $Ni_{80}Fe_{20}$ nanowire arrays have a strong (311) texture independent of the thickness. If glancing angle deposition is employed, the crystallographic low energy orientation of fcc materials tend to be inclined toward the flux direction,[1] and the texture along the normal to the substrate is determined by the degree of lattice match between the remaining planes and the seed layer (Cu(111)) plane, respectively.[2,4]. The lattice mismatch between the $Ni_{80}Fe_{20}$(311) plane and Cu(111) plane is 2.08%, much less than between the $Ni_{80}Fe_{20}$(220) or the $Ni_{80}Fe_{20}$(200) and the Cu(111) planes, respectively. In addition, the symmetry of the fcc(311) plane is nearly hexagonal.

Figure 2 shows the angular magnetization remanence of a 100 nm $Ni_{80}Fe_{20}$ sample. The sample magnetization was saturated at a magnetic field of 10 kOe, then the field was reduced to zero and the remanent magnetization was measured. This process was repeated for different angular orientations of the wire long axis relative to the magnetic field axis. The graph shows two local maxima around the directions that makes 25° relative to the [311] crystallographic directions, which is a little smaller than the angle that the $Ni_{80}Fe_{20}$ [111] crystallographic directions make with the [311] direction. The same procedure was repeated for several azimuthal orientations of the sample with identical results. This leads to the conclusion that the magnetization easy directions lie on the surface of a cone with some specific cone angle, similar to the crystallography of the low energy orientation.[1,8] This distribution was observed for thicknesses ranging between 50 and 150 nm. The relative difference in the remanent magnetization intensity between the easy axis and the local minima along the wire long axis decreases as the thickness increases. At about 200 nm deposited Permalloy, the shape anisotropy dominates and the magnetization easy axis points normal to the substrate plane along the wire's long axis.

Figure 3 shows the magnetization switching curves of the 100 nm $Ni_{80}Fe_{20}$ sample along the maximum remanent magnetization directions, the wire long axis and the in-plane magnetization hard direction. The remanent magnetization is larger toward some inclined direction (about 25° from the film normal), and the magnetization reaches saturation first along the wire's long axis. The in-plane curve also shows an abrupt switch at the coercive field. The samples with $Ni_{80}Fe_{20}$ thickness less than 50 nm showed a negative per-

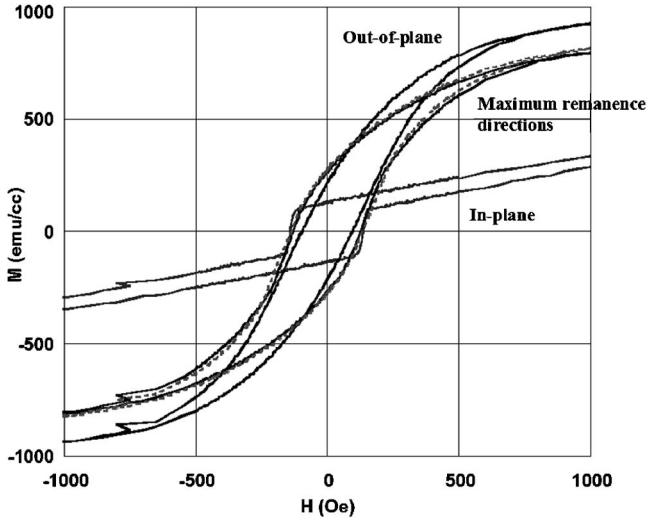

FIG. 3. Hysteresis loops for the 100 nm $Ni_{80}Fe_{20}$ sample. The magnetization approaches saturation first along the wire direction. Abrupt switching occurs in the in-plane directions at coercivity much lower than the saturation field.

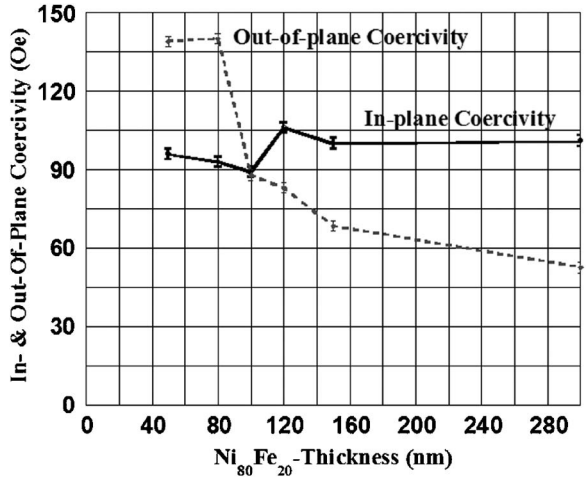

FIG. 4. In- and out-of-plane coercivities as functions of the $Ni_{80}Fe_{20}$ thickness. The in-plane coercivity remains almost constant, while the out-of-plane coercivity decreases with increasing thickness, crossing the in-plane coercivity at an aspect ratio of approximately one.

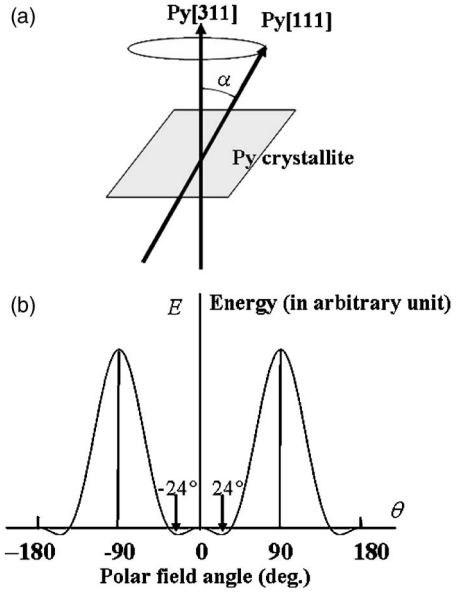

FIG. 5. (a) Schematic of the orientation distribution of $Ni_{80}Fe_{20}$ crystallites. The crystallites are distributed with their [311] axes along the film normal with the [111] axes distributed around it with an angle $\alpha=29.5°$. (b) The anisotropy energy E as a function of the magnetization angle Θ in a plane perpendicular to the substrate for the assumed biaxial anisotropy $E=K_1\sin^2\Theta+K_2\sin^4\Theta$ satisfying the conditions $K_1+2K_2>0$ and $K_1<0$. This model qualitatively explains the observed magnetic characteristics. $K_2/K_1=-3(K_1<0)$ is assumed, and E is in arbitrary units.

pendicular anisotropy and isotropic magnetization in the plane, and the samples with $Ni_{80}Fe_{20}$ thickness greater than 150 nm show perpendicular anisotropy.

Figure 4 shows the in- and out-of-plane coercivity as a function of deposited $Ni_{80}Fe_{20}$ thickness. At thicknesses between 80 and 120 nm, a strong decrease in the out-of-plane coercivity occurs while the in-plane coercivity remained relatively unchanged. This thickness range is approximately equal to the wire's diameter distribution of the same samples. At an aspect ratio of approximately one (using the average diameter) the in- and out-of-plane coercivities coincide at 90 Oe.

IV. DISCUSSION

The magnetic characteristics observed for the samples with a thickness less than 50 nm and greater than 150 nm are as expected, considering the procedure of the sample preparation and the crystallographic orientations described in Sec. III. However, the results obtained for the samples of the thickness between 50 and 150 nm, especially the double peaks obtained for the angular dependence of the remanence as shown in Fig. 2 and the characteristics of the hysteresis curves shown in Fig. 3, need some consideration.

A conceivable cause of these phenomena is a combination of the shape anisotropy of each grain composed of several crystallites exchange coupled with each other and the crystalline anisotropy corresponding to [111] axes uniformly distributed, on average, on a cone around the film normal [311] [Fig. 5(a)]. Macroscopically, this model with rotational symmetry around the film normal leads to a uniaxial anisotropy which can be generally expressed by

$$E = K_1 \sin^2 \theta + K_2 \sin^4 \theta, \tag{1}$$

to the fourth order, with θ denoting the magnetization angle with respect to the film normal. It is well known that this anisotropy shows double minima around the film normal, $\theta=0$, for

$$K_1 < 0, \quad K_1 + 2K_2 > 0, \tag{2}$$

which is called "conical anisotropy." This conical anisotropy model may explain the observed two maxima in the angular dependence of the remanent magnetization shown in Fig. 2. However, in order to explain the characteristic features of the hysteresis curves shown in Fig. 3, we should modify the above macroscopic model. If we assume each grain contains anisotropy expressed by the same formula as in Eqs. (1) and (2) with the restriction that the magnetizations are confined within a plane including the common [311] axis vertical to the film plane, most of the magnetic features shown in Figs. 2 and 3 can be reproduced at least qualitatively.

This kind of anisotropy is biaxial in the vertical plane, and may be generated by assuming that each grain consists of a pair of crystallites whose [111] axes are aligned symmetrically with respect to the [311] axis. In Fig. 5(b), an example of the anisotropy energy as a function of the angle θ is shown, where $K_2/K_1=-3$ is assumed. The characteristic of this type of anisotropy is that it shows a local maximum at $\theta=0$ with double minima around it at $\theta=\pm\theta_0$, with θ_0 expressed as

$$\theta_0 = \sin^{-1}\sqrt{\frac{-K_1}{2K_2}}, \tag{3}$$

which gives about 24° for the example above. According to this kind of anisotropy, the abrupt switch of the magnetization at a relatively low coercive field H_c in the in-plane hys-

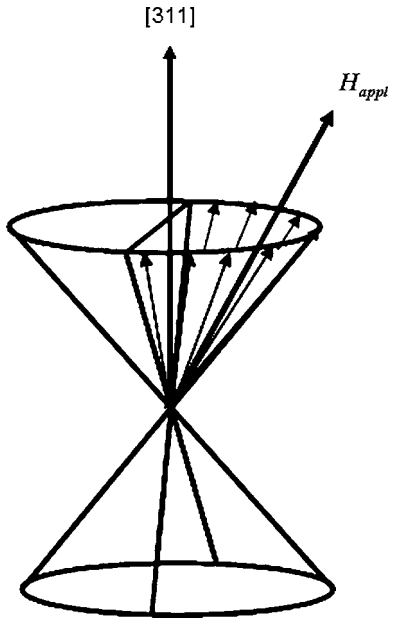

FIG. 6. Remanent magnetization states: the arrows distributed in the conical plane indicate the distribution of the remanent magnetization after the saturating field H_{appl} is applied. If H_{appl} is applied along the opposite side of the film normal in the plane which [311] and H_{appl} makes, the remanent magnetizations make a symmetric distribution with respect to [311].

teresis curve is ascribed to the switching between the two local minima around $\theta=0$. The extremely high saturation field H_s in the in-plane direction, compared to H_c, obtained by extrapolation of the slope at zero applied field can be understood by assuming an appropriate value for the ratio $|K_2/K_1|$, because H_s/H_c goes as $\sim|K_2/K_1|^{3/2}$ for the large $|K_2/K_1|$ value (see the Appendix).

The double peaks observed in the angular dependence of the remanence can also be explained with biaxial anisotropy similar to the case of conical anisotropy. In this case, however, the remanent magnetizations will make a distribution on the surface of a double conical surface. A typical ideal remanent state is shown schematically in Fig. 6. The only direction along which the magnetization can saturate at a finite field is the film normal direction. In the actual situation, due to the dispersion in anisotropy and the macroscopic demagnetizing effect, the magnetization of some of the grains may switch to the opposite direction with respect to the film plane, reducing the vertical component of the average remanent magnetization. This illustrates how the magnetization reaches saturation first in the perpendicular direction rather than in the maximum remanence direction, and the relatively low remanent magnetization in every direction.

What is puzzling, however, is the origin of the above anisotropy. In order to explain the observed in-plane coercivity ($\sim$135 Oe) and saturation field ($\sim$4000 Oe), the above model requires K_1 and K_2 on the order of 10^5-10^6 erg/cc, which is too large to be ascribed to the crystalline anisotropy of ordinary $Ni_{80}Fe_{20}$. Furthermore, in order to attribute the biaxial nature to the crystalline anisotropy, the [111] axis may have to be an easy direction. This is opposite to bulk $Ni_{80}Fe_{20}$, for which the [111] axis is a hard direction. The shape anisotropy is probably too weak to explain the origin of the anisotropy, since each crystallite of the samples of the thickness ranging between 50 and 150 nm is not elongated enough to give the order of 10^6 erg/cc anisotropy.

The continuous decrease in the out-of-plane coercivity at thicknesses higher than 150 nm shown in Fig. 4 may be due to the increase in the wire diameter, which also leads to a more continuous film at some parts of the sample making the in-plane direction increasingly magnetically easier. The cause of the observed constant H_c at an aspect ratio of approximately one is also a matter of further investigation.

V. CONCLUSIONS

In this work, we studied the effect of the crystallography on the magnetic properties of $Ni_{80}Fe_{20}$ deposited on epitaxial Cu(111) nanoarrays on the magnetic anisotropy. The angular remanence of samples with thicknesses on the order of the average wire diameter showed that the easy axes are uniformly distributed on the surface of a cone. This and other observed magnetic characteristics are found to be qualitatively explained by a model which includes biaxial anisotropy for each grain, the origin of which needs to be further investigated. Magnetization switching curves show that the samples saturate first along the wire direction, while the in-plane direction constitutes the sample magnetic hard axis. At an aspect ratio of approximately one, the in- and out-of-plane coercivites coincide.[9]

ACKNOWLEDGMENTS

This work was funded by Grant Nos. NSF-ECS-0331864 and NSF-DMR-0213985.

APPENDIX

The energy of the system is given by

$$E = K_1 \sin^2\theta + K_2 \sin^4\theta - M_s H \sin\theta, \tag{A1}$$

where K_1 and K_2 are the anisotropy constants, θ is the magnetization angle with respect to the vertical direction, M_s is the saturation magnetization, and H is the applied field in the plane which includes the two out-of-plane [111] axes. Normalizing this expression by $-K_1$, we obtain

$$w = -\sin^2\theta + k\sin^4\theta - 2h\sin\theta, \tag{A2}$$

where $w=-E/K_1$, $k=-K_2/K_1$, and $h=H/H_{k1}$ with $H_{k1}=-2K_1/M_s$. The coercivity h_c at which the magnetization switches abruptly from one energy minimum to the other found from the critical conditions:

$$\frac{dw}{d(\sin\theta)} = 0 \tag{A3}$$

and

$$\frac{d^2w}{d(\sin\theta)^2} = 0, \tag{A4}$$

which leads to the expression

$$h_c = \frac{2}{3}\sqrt{\frac{1}{6k}}. \tag{A5}$$

In addition, the saturation field is found from substituting $\sin\theta = 1$ into Eq (A3), which leads to

$$h_s = 2k - 1. \tag{A6}$$

The ratio h_s/h_c is then

$$\frac{h_s}{h_c} = \tfrac{3}{2}(2k-1)\sqrt{6k}, \tag{A7}$$

and finally

$$\lim_{k\to\infty} \frac{h_s}{h_c} = 3\sqrt{6}\cdot k^{3/2}. \tag{A8}$$

[1]H. Alouach and G. J. Mankey, J. Vac. Sci. Technol. A **22**, 1379 (2004).
[2]H. Alouach and G. J. Mankey, J. Mater. Res. **19**, 3620 (2004).
[3]H. Alouach and G. J. Mankey, Appl. Phys. Lett. **86**, 123114 (2005).
[4]P. ten Berge, L. Abelmann, J. C. Lodder, A. Schrader, and S. Luitjens, J. Magn. Soc. Jpn. **18**, 295 (1994).
[5]M. Suzuki and Y. Taga, J. Appl. Phys. **71**, 2848 (1992).
[6]F. Liu, M. T. Umlor, L. Shen, J. Weston, W. Eads, J. A. Barnard, and G. J. Mankey, J. Appl. Phys. **85**, 5486 (1999).
[7]T. Karabacak, G.-C. Wang, and T.-M. Lu, J. Vac. Sci. Technol. A **22**, 1778 (2004).
[8]T. Karabacak, A. Mallikarjunan, J. P. Singh, D. Ye, G. Wang, and T. Lu, Appl. Phys. Lett. **83**, 3096 (2003).
[9]J. D. Kleis, Phys. Rev. **50**, 1178 (1936).